ACS APPLIED MATERIALS & INTERFACES

www.acsami.org

Research Article

Replacement of Concrete Aggregates with Coal-Derived Flash Graphene

Paul A. Advincula, Wei Meng, Lucas J. Eddy, Phelecia Z. Scotland, Jacob L. Beckham, Satish Nagarajaiah,* and James M. Tour*

Cite This: *ACS Appl. Mater. Interfaces* 2024, 16, 1474−1481

Read Online

ACCESS | Metrics & More | Article Recommendations | Supporting Information

ABSTRACT: Each year, the growth of cities across developing economies in Asia, Africa, and Latin America drives demand for concrete to house and serve their burgeoning populations. Since 1950, the number of people living in urban areas has quadrupled to 4.2 billion, with another predicted 2.5 billion expected to join them in the next three decades. The largest component of concrete by volume is aggregates, such as sand and rocks, with sand as the most mined material in the world. However, the extraction rate of sand currently exceeds its natural replenishment rate, meaning that a global concrete-suitable sand shortage is extremely likely. As such, replacements for fine aggregates, such as sand, are in demand. Here, flash Joule heating (FJH) is used to convert coal-derived metallurgical coke (MC) into flash graphene aggregate (FGA), a blend of MC-derived flash graphene (MCFG), which mimics a natural aggregate (NA) in size. While graphene and graphene oxide have previously been used as reinforcing additives to concrete, in this contribution, FGA is used as a total aggregate replacement for NA, resulting in 25% lighter concrete with increases in toughness, peak strain, and specific compressive strength of 32, 33, and 21%, respectively, with a small reduction in specific Young's modulus of 11%. FJH can potentially enable the replacement of fine NA with FGA, resulting in lighter, stronger concrete.

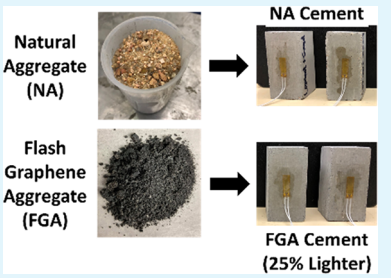

KEYWORDS: *flash Joule heating, flash graphene, concrete, aggregate replacement, construction materials*

1. INTRODUCTION

Concrete is the second most consumed material worldwide, after water.[1,2] Its ease of use and impressive mechanical properties have literally laid the foundation for modern civilization. Concrete usage is twice that of steel, wood, plastics, and aluminum combined.[1] Typically, concrete is composed of fine or coarse aggregates, such as sand or gravel, which are bonded with cement and water and cured over time.[3] However, production of concrete imposes substantial environmental impacts, through both production of cement and the use of aggregates.

Cement production accounts for 8% of worldwide CO_2 emissions, primarily due to the thermal decomposition of calcium carbonate to generate metal oxides and CO_2 and the fossil fuels combusted during the process.[4,5] Production of 1 t of Portland cement emits 0.9 t of CO_2.[6]

Meanwhile, the use of sand from riverbeds and deltas as aggregates in concrete also presents noteworthy environmental issues. Sand mining erodes coastlines, destroys aquatic life, and threatens local communities. Nearly 50 billion tons of sand are extracted each year, making it the most mined material in the world.[7] The use of sand has tripled over the past two decades as the demand for concrete rises from developing countries building new infrastructure.[8] Despite its widespread use, the extraction impacts of sand are not well-understood, and extraction rates exceed natural sand replenishment rates.[9] Unless change is found, the world may very soon be facing a shortage of its most mined material.[10] Potential replacements for fine aggregates have been examined, including waste foundry sand,[11,12] oyster shells,[10] waste glass sand,[13] coconut shell,[14] and rubber-like materials.[15] However, replacement with these materials generally has a negative impact on the mechanical properties of the final concrete.

Recently, our research group demonstrated that flash Joule heating (FJH) could be used to synthesize flash graphene (FG) from a variety of different feedstocks, including waste plastic,[16−18] coffee grounds,[19] asphaltenes,[20] soybean oil,[21] and rubber tires.[22] The resulting FG is turbostratic[23] and more easily dispersed in composites than graphene produced from exfoliation of graphite.[24] A variety of other applications have been explored for FJH, including synthesis of hybrid carbon nanomaterials,[25,26] doped materials,[27−29] anode recycling,[30] and heavy metal removal from coal fly ash.[31] Coal materials have been demonstrated to be excellent feedstocks for FG due to their high carbon content. As renewable energy sources become more ubiquitous, the annual consumption of coal is estimated to fall from 5.25 billion tons in 2020 to 600 million

Received: October 10, 2023
Revised: December 6, 2023
Accepted: December 13, 2023
Published: December 29, 2023

Scheme 1. (a) Scheme Depicting the Preparation of FGA and Subsequent Replacement of NA for Casting of Concrete and (b) Composition of Size Proportions in NA and FGA[a]

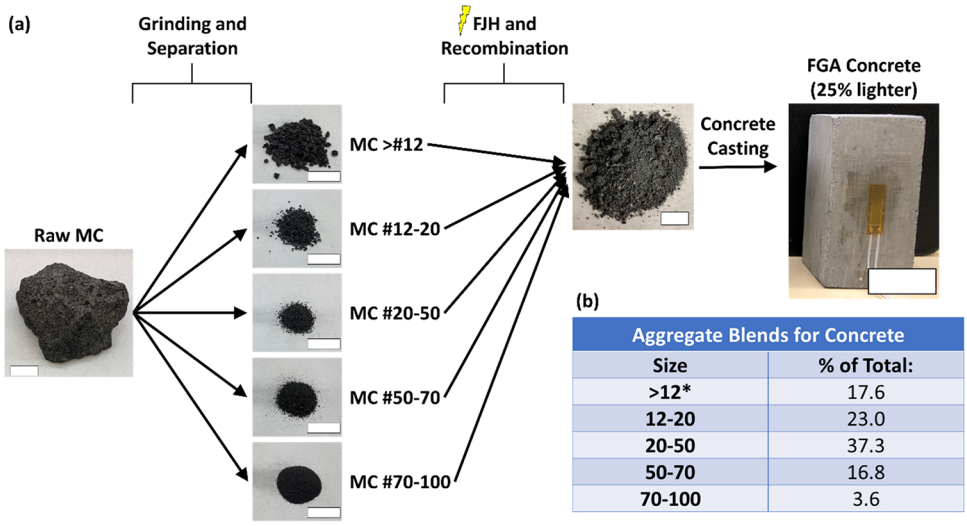

(b)

Aggregate Blends for Concrete	
Size	% of Total:
>12*	17.6
12-20	23.0
20-50	37.3
50-70	16.8
70-100	3.6

[a]All scale bars are 2 cm. The tan rectangular probe with two wires attached to the FGA concrete sample is a strain gauge. *The grain size is larger than mesh size 12, indicating a smaller grain number.

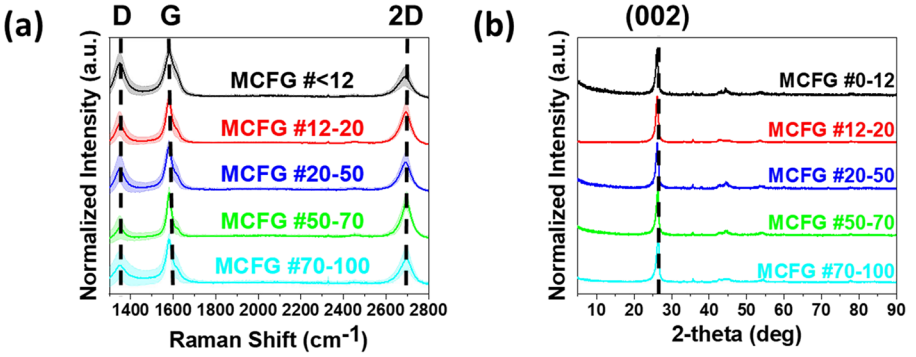

(c)

Sample & Size:	I_{2D}/I_G Ratio:	I_D/I_G Ratio:	Graphene Yield (%):	(002) Peak Position:
MCFG >#12 (>1.68 mm)	0.585	0.400	100	26.08°
MCFG #12-20 (1.68 - 0.841 mm)	0.557	0.473	100	26.14°
MCFG #20-50 (0.841 - 0.297 mm)	0.556	0.388	100	26.18°
MCFG #50-70 (0.297 - 0.210 mm)	0.525	0.418	98.9	26.34°
MCFG #70-100 (0.210 - 0.149 mm)	0.518	0.377	92.7	26.44°

Figure 1. (a) Average Raman spectra with standard deviation shown as the shaded regions and (b) XRD characterization of FGA. (c) Yield data and (002) peak analysis of different particle sizes in FGA.

tons in 2050.[32] Hence, coal producers are eager to find alternative applications for coal materials. Metallurgical coke (MC), a coal-based product, has been demonstrated by our group to be one of the best feedstocks for conversion due to its high carbon content, coupled with its high conductivity.[33−35] In 2018, nearly 639.22 Mt of MC was produced, predominantly for use in the steel industry.[36] While these reserves are currently smaller than that of concrete-suitable sand, this market will likely continue to grow as demand for steel increases.[37,38] As demand for concrete increases and the rate of sand extraction further outpaces the natural replenishment rate of sand, reserves of concrete-suitable sand will continue to

https://doi.org/10.1021/acsami.3c15156
ACS Appl. Mater. Interfaces 2024, 16, 1474−1481

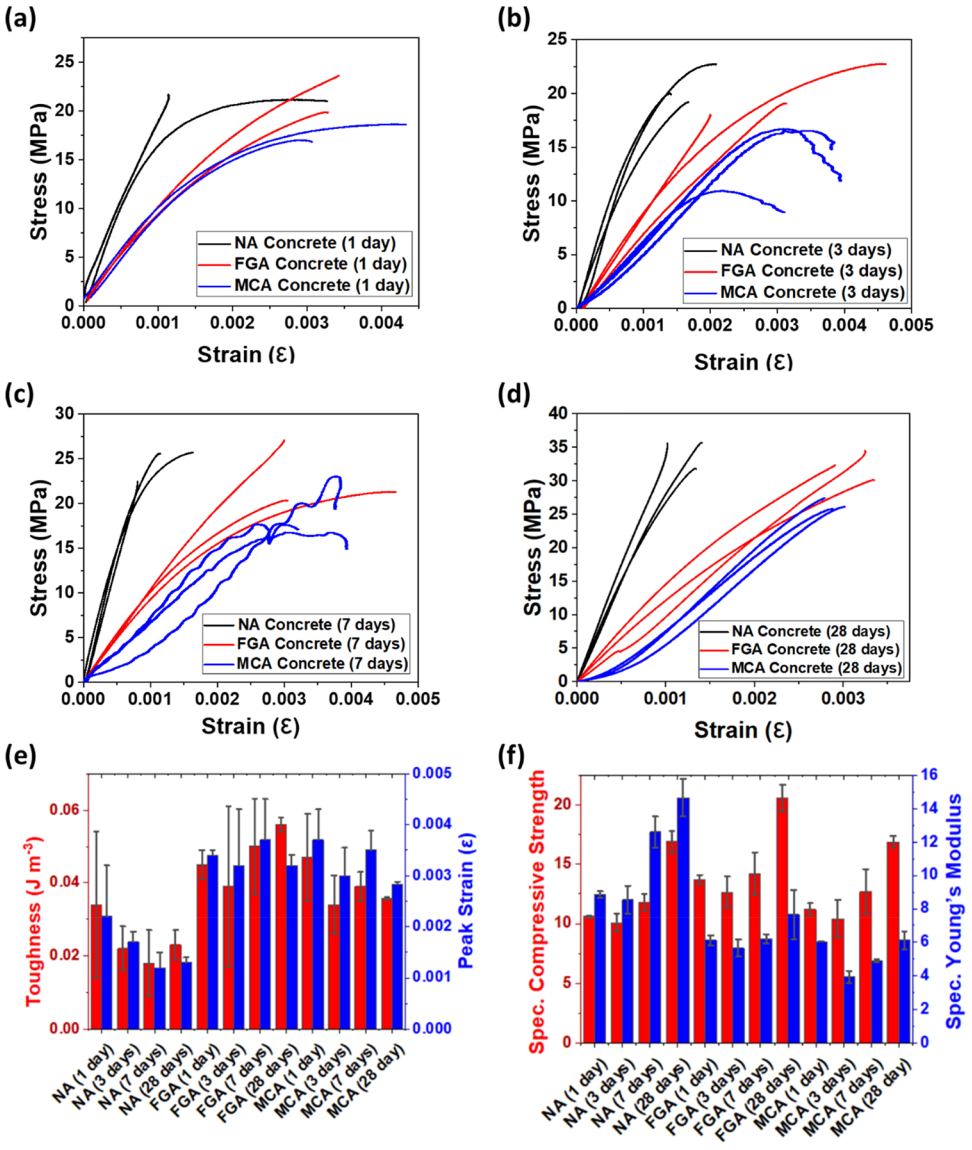

Figure 2. Comparison of compressive stress−strain curves of FGA, MCA, and NA concrete at (a) 1, (b) 3, (c) 7, and (d) 28 days of curing. The cement:aggregate volume ratio is 1.0, and the water:cement mass ratio is 0.6. (e,f) Comparison of mechanical properties of concrete samples made with FGA, MCA, and NA. The units of specific compressive strength are kPa m^3 kg^{-1}, and the units of specific Young's modulus are MPa m^3 kg^{-1}.

dwindle. As such, finding aggregate alternatives to sand has become increasingly important.

Here, we demonstrate the use of MC-derived FG (MCFG) as both a reinforcing additive in cement and a potential replacement for fine aggregates in concrete. MC is also favorable for this application due to its large particle size relative to FG formed from other feedstocks,[33] which leads to a similar grain size profile found in concrete made with traditional natural aggregates (NA). A blend of MCFG is prepared with size proportions similar to NA, resulting in flash graphene aggregate (FGA). This FGA is used here as a total replacement for NA, resulting in lighter concrete with increased toughness, peak strain, and specific compressive strength, along with only a small reduction in specific Young's modulus. FGA can potentially be used to lighten and strengthen concrete while also replacing, in part, our dwindling reserves of concrete-suitable sand with carbon-based materials from coal.

2. RESULTS AND DISCUSSION

To mimic the size and composition of NA with FGA, raw MC was ground using a grinder (Goldbelt Global, model OS0411CSVS, serial no. oSEL04110091, 110 V) to achieve the same size proportions as NA (Scheme 1a) as per ASTM C33 (American Society for Testing and Materials) specifications. NA was separated into different sizes with sieves of varying meshes ranging from #12 to #100. Each size proportion was weighed to determine the percent of the aggregate that each size comprised (Scheme 1b). After grinding, the MC was separated into the same size proportions and FJH into MCFG. Peak currents during this process range from ∼1592 to ∼890 A, generally decreasing as the particle size decreases (Figure S1). In 2021, the average cost of 1 t of MC was $234.[39] The industrial rate for electricity in Texas is ∼$0.04 kW h^{-1}, so the cost of converting MC into MCFG ranges between ∼$71 and $84 per ton (Figure S2). Energy density was reduced for the two smallest size portions since higher voltages produce lower-quality FG with smaller

https://doi.org/10.1021/acsami.3c15156
ACS Appl. Mater. Interfaces 2024, 16, 1474−1481

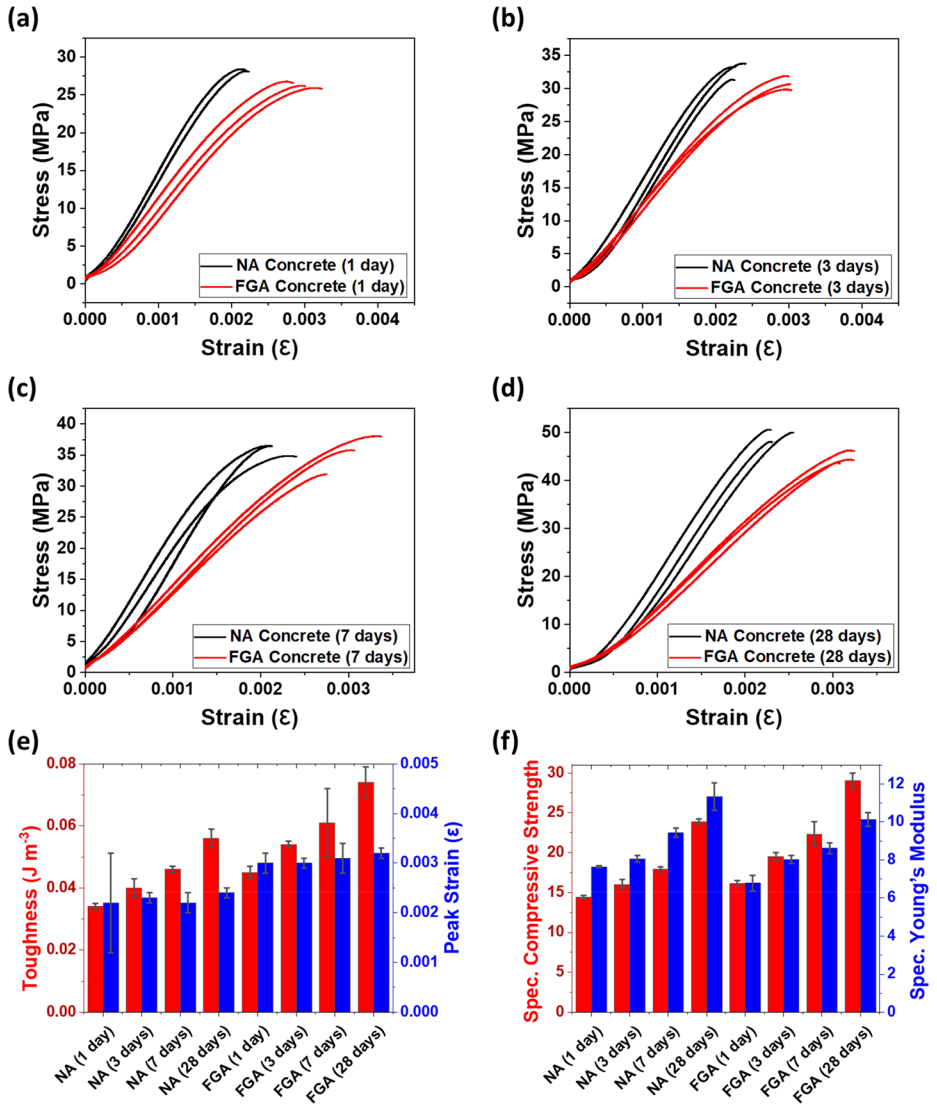

Figure 3. Comparison of compressive stress−strain curves of FGA, MCA, and NA concrete at (a) 1, (b) 3, (c) 7, and (d) 28 days of curing. The cement:aggregate volume ratio is 1.0, and the water:cement mass ratio is 0.5. (e,f) Comparison of mechanical properties of concrete samples made with NA and FGA. The units of specific compressive strength are kPa m^3 kg^{-1}, and the units of specific Young's modulus are MPa m^3 kg^{-1}.

particles. These varying sizes were recombined into FGA using the measured proportions of NA. FGA was then used as a total replacement for NA in concrete, reducing the average sample weight by 25%, due to the lower density of FGA (Figure S3).

Raman spectroscopy and XRD are powerful tools for assessing the quality and turbostraticity of graphene as seen in Figure 1.[19] Raman spectroscopy can be used to determine quality through analysis of the D, G, and 2D peaks that appear at ∼1350, ∼1580, and ∼2700 cm^{-1}, respectively. In Figure 1a, the average of 100 different Raman spectra is presented for each size of particle present in the FGA blend. Graphene yield is defined as the percentage of spectra that can be classified as graphene based on meeting the following criteria: (1) an I_{2D}/I_G ratio of ≥0.3, (2) a signal-to-noise ratio of >5 in the 2D band region, and finally, (3) a 2D band fwhm of <100 cm^{-1}. The graphene yield for each size proportion of FGA was found to be >90% with an average I_{2D}/I_G ratio greater than 0.5, indicating that the MCFG used as FGA is of good quality. Generally, a high I_{2D}/I_G ratio is desirable since it is indicative of extended 2D material properties. A lower I_D/I_G ratio indicates that fewer defects and graphene edges are present.

XRD also provides insight into the turbostraticity of the FG, as seen in Figure 1b. FG has been shown to be turbostratic, meaning that the sheets of graphene are rotated about the axis normal to the sheet below, resulting in an increased interlayer spacing and decreased interlayer electron transport, enabling retention of 2D material properties even with an increased number of layers.[19] This rotation contrasts with AB stacking that appears in conventionally produced graphene from graphite exfoliation, where electron-deficient areas are stacked on top of electron-rich areas. The AB stacking leads to increased interlayer electron transport and a shift to 3D material properties as the number of layers increases. Further, AB-structured graphene is harder to exfoliate in composites due to the strong interlayer interactions. The decrease in the diffraction angle and the increase in fwhm of the (002) peak are some of the best indicators of turbostraticity found in FG. Here, we see that the smallest sizes of MCFG (#70−100) have a (002) peak position of 26.44°. This value is close to that of AB-stacked graphene, which is 26.4°, indicating increasing AB stacking of this size proportion of MCFG. Increasing sizes of MCFG show a downward shift in the (002) peak position,

https://doi.org/10.1021/acsami.3c15156
ACS Appl. Mater. Interfaces 2024, 16, 1474−1481

with the lowest value being 26.08°, indicating that the larger sizes of MCFG are more turbostratic.

Initial testing of NA concrete and FGA concrete was conducted at a cement:aggregate volume ratio of 1.0 and a water:cement mass ratio of 0.6, as seen in Figure 2. After 1 day of curing, concrete made with NA, FGA, and metallurgical coke aggregate (MCA) was compared through compressive testing (Figure 2a). MCA is made up of MC in the same size proportions as NA, prior to FJH conversion into FGA. Given that FGA concrete is 25% lighter than NA concrete, rather than reporting compressive strength and Young's modulus, the specified versions of each are reported. These consider the density of the material, thereby providing a stiffness to mass ratio.[40,41] Here, toughness is measured by calculating the area under each stress−strain curve by using the Integrate function of Origin software. All values for toughness, peak strain, compressive strength, Young's modulus, specific compressive strength, and specific Young's modulus can be found in Table S1.

After 1 day, FGA concrete has 32, 54, and 29% increases in toughness, peak strain, and specific compressive strength, respectively, compared to NA concrete (Figure 2e,f). However, it has a 31% lower specific Young's modulus. This decrease in Young's modulus is likely due to the decreased hardness of the FGA compared to NA. MCA concrete has 38, 68, and 6% increases in toughness, peak strain, and specific compressive strength, respectively, compared to NA concrete. However, it also shows a 32% decrease in specific Young's modulus. Given the importance of compressive strength and Young's modulus, FGA is preferable for use over MCA. This could potentially be due to the enhanced dispersibility of FG compared to the amorphous carbon feedstocks used in its production.[19] Here, raw compressive strength and Young's modulus of NA concrete are higher than those of FGA and MCA concrete. Again, as NA concrete is significantly heavier than FGA and MCA concrete, the specific compressive strength and specific Young's modulus are used to compare the strength-to-weight ratios, rather than the simple compressive strength and Young's modulus.

Extending the curing time from 1 day to 3, 7, and 28 days shows similar trends in the comparison between NA concrete and FGA concrete, where toughness, peak strain, and specific compressive strength of FGA concrete are comparable or higher than in NA concrete (Figure 2b−d). As the curing time increases, the properties of MCA concrete fall further behind those of FGA concrete and NA concrete. MCA without FJH results in a poorer performing aggregate replacement than FGA. Hence, MCA is not used in further testing for water:cement ratio optimization.

The increase in mechanical properties when comparing FGA concrete to MCA concrete can potentially be attributed to the formation of powerful interfacial forces between carboxylic groups and hydration products, enhanced mechanical interlocking, or promotion of hydration processes.[42,43] These microscale processes appear when graphene is used as a reinforcing additive and are likely also present when FGA is used as an aggregate. These processes would not be present in MCA concrete where MCA is mixed prior to FJH as MCA is amorphous. Sheets of FG are likely dispersed in the cement during the curing stages of FGA concrete, leading to these effects, as well as the filler effect for acceleration of hydration reactions for cementitious materials and the bridging effect of graphene nanoplatelets for microcracks.[44,45] However, further study is necessary to fully elucidate the mechanisms at work.

Since concrete strength is tied to the ratio of water and cement, we studied this relationship in concrete made with FGA. Testing of NA concrete and FGA concrete was conducted at a cement:aggregate volume ratio of 1.0 and a water:cement mass ratio of 0.5, as seen in Figure 3. All values for toughness, peak strain, compressive strength, Young's modulus, specific compressive strength, and specific Young's modulus can be found in Table S2. The compressive strength values observed mean that these materials could be suitable for most types of concrete construction, aside from high-rise buildings and columns.[46] Similar trends are observed in FGA concrete, where toughness, peak strain, and specific compressive strength are comparable to or higher than NA concrete, at the cost of specific Young's modulus (Figure 3). At 28 days, toughness, peak strain, and specific compressive strength of FGA concrete are 32, 33, and 21% higher than those of NA concrete, respectively (Figure 3e,f). However, at this water:cement mass ratio, the specific Young's modulus of FGA concrete is much closer to that of NA concrete, with 11, 0.4, 8.7, and 11% reductions at 1, 3, 7, and 28 days, respectively, as each sample achieves its maximum strength after 28 days.

Moving forward, a variety of experiments studying the effects of graphene aggregates on cement hydration and densification could be carried out to better understand the mechanisms behind the use of FGA. Experiments such as hydration heat, pore structure analysis, and the measurement of water absorption might elucidate these mechanisms. Additionally, the unique properties of FGA might lead to an additional functionality such as self-sensing.

3. CONCLUSIONS

Here, FGA is prepared through FJH of MC into high-quality turbostratic FG with varying sizes, according to the makeup of NA. This FGA is demonstrated for use as a replacement for fine NA, such as sand, reducing the deleterious effects of sand removal from its natural environment. FGA in concrete enables a 25% reduction in weight, along with increases in toughness, peak strain, and specific compressive strength of 32, 33, and 21%, respectively, with slight reductions in specific Young's modulus. As demand for sand worldwide continues to outpace its natural replenishment rates, the use of FJH to prepare FGA from coal-derived materials can enable replacement of fine sand aggregates. Finally, since the weight of the FGA-based concrete is 25% less than that of the NA-based concrete, significant savings on transportation to the construction site will be realized.

4. EXPERIMENTAL SECTION/METHODS

4.1. Materials. MCFG was prepared by sieving ground MC and FJH of the varying portions of MC size. NA was found to be composed of particles with sizes ranging from larger than mesh size #12 to #100. Of the NA particles measured, 17.6% were > #12 (>1.68 mm), 23.0% were #12−20 (1.68−0.841 mm), 37.3% were #20−50 (0.841−0.297 mm), 16.8% were #50−70 (0.297−0.210 mm), and 3.6% were #70−100 (0.210−0.149 mm) (Scheme 1). Particles of MC were separated using the sieves, and each individual size of MC was subjected to a variable FJH pulse with duty cycles of 10, 20, and 50%, for 1, 0.5, and 5 s, respectively. Depending on the size of the MC feedstock, pulses of 350, 370, or 380 V and a 1,000 Hz frequency were used to produce MCFG (Figures S1 and S2). Using the measured proportions for NA, different size proportions of MCFG were

https://doi.org/10.1021/acsami.3c15156
ACS Appl. Mater. Interfaces 2024, 16, 1474−1481

combined into a blend of FGA that mimics the size distributions of NA. Quikrete all-purpose sand was used as NA.

4.2. Raman Spectroscopy. Raman spectra were collected with a Renishaw inVia confocal Raman microscope and a 532 nm laser. A 50× objective lens was used with a laser power of 5 mW to scan the samples from 1300 to 2800 cm^{-1}. Large-area Raman mapping was used to determine the crystallinity and morphology of the FG with analysis of the spectra using a custom-written Python script from the RamPy package. Collected spectra were background-corrected, and a Savitsky−Golay filter was used to smooth the spectra before quantification of graphene yield and peak ratios. To qualify as graphene, three criteria were used to assess individual spectra: (1) a minimum I_{2D}/I_G ratio of 0.3, (2) a signal-to-noise ratio of >5 in the 2D band region, and (3) a 2D band with an fwhm of <100 cm^{-1}. To minimize variation in the *z*-height during collection of large-area Raman maps, each sample of MCFG was ball-milled at 400 rpm for 2 h into a fine powder.

4.3. X-ray Diffraction (XRD). XRD data of ball-milled MCFG were collected and analyzed on a Rigaku SmartLab II instrument with zero-background sample holders. Collection was carried out with a scan width of 0.02° $step^{-1}$ and a scan rate of 2° min^{-1}.

4.4. Concrete Mix Design. The cement used in this project was Portland cement type I/II manufactured with ASTM C150 specifications. The sizes of NA used in concrete mixing followed ASTM C33 specifications. For NA concrete specimens, the cement/aggregate weight ratio was 0.5, which was used for common purpose concrete mixing. Because the density of FGA was ∼0.7 g cm^{-3}, which is approximately half of the density of the NA, the FGA concrete can be filled by FGA with half the weight of NA that would be required to occupy the same volume. We started with a 0.4 water/cement ratio and observed reduced workability in concrete with FGA or MCA. Compared to NA concrete, the FGA and MCA concrete samples have a higher segregation of aggregates and lower flowability. It was difficult to maintain the homogeneity of the concrete mix. For this reason, we increased the water/cement ratio to 0.5 and then to 0.6 to increase the workability. At this stage of study, no superplasticizer was added in the concrete mix, though this could be attempted in future work. Additionally, FGA and NA were not used in combination; instead, the effect of total replacement of NA with FGA is shown here.

4.5. Compressive Testing. All concrete specimens were removed from the molds after 24 h and then cured in water for 1, 3, 7, and 28 days. Because of the limitation of the FGA production, the size of the concrete specimen was proportionally scaled down based on the ASTM C39 specifications. The ASTM standard specimen was a 101.6 × 203.2 mm^2 cylinder. The dimensions of the concrete specimen used in this study were 25.4 × 25.4 × 50.8 mm^3. To perform an ASTM standard test, 200 times as much volume would need to be filled with FGA, which was not feasible with laboratory-scale production of FGA. Moving forward, larger production facilities will likely enable us to test larger specimen sizes. The specimens were tested on a uniaxial compression machine with a 0.002 in min^{-1} loading rate. The load and strain were recorded by a loading cell and an attached strain gauge, respectively.

■ ASSOCIATED CONTENT

Supporting Information

The Supporting Information is available free of charge at https://pubs.acs.org/doi/10.1021/acsami.3c15156.

Representative curves of current as a function of time during FJH of FGA, energy density and FJH data for preparation of FGA, preparation of concrete samples with NA and FGA, and compressive stress−strain data (PDF)

■ AUTHOR INFORMATION

Corresponding Authors

Satish Nagarajaiah − *Department of Civil and Environmental Engineering, Rice University, Houston, Texas 77005, United States; Smalley-Curl Institute, NanoCarbon Center, and the Rice Advanced Materials Institute, Rice University, Houston, Texas 77005, United States; Department of Materials Science and NanoEngineering, Rice University, Houston, Texas 77005-1892, United States; Department of Mechanical Engineering, Rice University, Houston, Texas 77005, United States*; Email: satish.nagarajaiah@rice.edu

James M. Tour − *Department of Chemistry, Rice University, Houston, Texas 77005-1892, United States; Smalley-Curl Institute, NanoCarbon Center, and the Rice Advanced Materials Institute, Rice University, Houston, Texas 77005, United States; Department of Materials Science and NanoEngineering, Rice University, Houston, Texas 77005-1892, United States*; orcid.org/0000-0002-8479-9328; Email: tour@rice.edu

Authors

Paul A. Advincula − *Department of Chemistry, Rice University, Houston, Texas 77005-1892, United States*; orcid.org/0000-0002-2838-0696

Wei Meng − *Department of Civil and Environmental Engineering, Rice University, Houston, Texas 77005, United States*

Lucas J. Eddy − *Department of Chemistry, Rice University, Houston, Texas 77005-1892, United States; Smalley-Curl Institute, NanoCarbon Center, and the Rice Advanced Materials Institute and Applied Physics Program, Rice University, Houston, Texas 77005, United States*

Phelecia Z. Scotland − *Department of Chemistry, Rice University, Houston, Texas 77005-1892, United States; Department of Materials Science and NanoEngineering, Rice University, Houston, Texas 77005-1892, United States*

Jacob L. Beckham − *Department of Chemistry, Rice University, Houston, Texas 77005-1892, United States*

Complete contact information is available at: https://pubs.acs.org/10.1021/acsami.3c15156

Notes

The authors declare the following competing financial interest(s): Rice University owns the intellectual property (IP) on the process to generate flash graphene. Universal Matter Inc. has licensed that IP from Rice University. JMT is a stockholder in that company, but not an officer, director, or employee. The specific use of FGA in concrete has been protected by patent application filing, and that IP remains unlicensed. Conflicts of interest are mitigated through compliance and reporting with the Rice University Office of Sponsored Programs and Research Compliance.

■ ACKNOWLEDGMENTS

We thank the US Army Corps of Engineers, ERDC (W912HZ-21-2-0050) and the Air Force Office of Scientific Research (FA9550-22-1-0526) for their support. J.L.B. acknowledges support from the NSF Graduate Research Fellowship Program.

■ REFERENCES

(1) Gagg, C. R. Cement and Concrete as an Engineering Material: An Historic Appraisal and Case Study Analysis. *Eng. Fail. Anal.* **2014**, *40*, 114−140.

(2) Myers, M. D.; Kempthorne, D. *Mineral Commodity Summaries 2007*, U.S. Geological Survey 2007.
(3) *How Concrete is Made* https://www.cement.org/cement-concrete/how-concrete-is-made.
(4) Flatt, R. J.; Roussel, N.; Cheeseman, C. R. Concrete: An Eco Material That Needs to Be Improved. *J. Eur. Ceram. Soc.* **2012**, *32*, 2787−2798.
(5) WBCSD. *The Cement Sustainability Initiative: Our Agenda for Action*. 2002.
(6) Portland Cement Association. *Carbon Footprint: What Is It?* Portland Cement Association 0020−11−105 8−9.
(7) Koehnken, L. *Impacts of Sand Mining on Ecosystem Structure, Process & Biodiversity in Rivers* Fact Sheet/Executive Summary, WWF; 2018.
(8) United Nations Environment Programme. *Rising Demand for Sand Calls for Resource Governance*. 2019, 3−8.
(9) UN Environment Programme. *Sand and Sustainability: 10 Strategic Recommendations to Avert a Crisis*; 2022.
(10) Yang, E. I.; Kim, M. Y.; Park, H. G.; Yi, S. T. Effect of Partial Replacement of Sand with Dry Oyster Shell on the Long-Term Performance of Concrete. *Constr. Build. Mater.* **2010**, *24*, 758−765.
(11) Ashish, D. K.; Verma, S. K.; Ju, M.; Sharma, H. High Volume Waste Foundry Sand Self-Compacting Concrete − Transitioning Industrial Symbiosis. *Process Saf. Environ. Prot.* **2023**, *173*, 666−692.
(12) Ashish, D. K.; Verma, S. K. Robustness of Self-Compacting Concrete Containing Waste Foundry Sand and Metakaolin: A Sustainable Approach. *J. Hazard. Mater.* **2021**, *401*, No. 123329.
(13) Tamanna, N.; Tuladhar, R.; Sivakugan, N. Performance of Recycled Waste Glass Sand as Partial Replacement of Sand in Concrete. *Constr. Build. Mater.* **2020**, *239*, No. 117804.
(14) Animesh, K.; Tiwari, J.; Soni, K. Partial Replacement of Fine Aggregate & Coarse Aggregate by Waste Glass Powder & Coconut Shell. *Int. Res. J. Eng. Technol.* **2017**, *6*, 369−376.
(15) Supar, K.; Rani, F. A. A.; Mazlan, N. L.; Musa, M. K. Partial Replacement of Fine Aggregate Using Waste Materials in Concrete as Roof Tile: A Review. *IOP Conf. Ser. Mater. Sci. Eng.* **2021**, *1200*, No. 012008.
(16) Algozeeb, W. A.; Savas, P. E.; Luong, D. X.; Chen, W.; Kittrell, C.; Bhat, M.; Shahsavari, R.; Tour, J. M. Flash Graphene from Plastic Waste. *ACS Nano* **2020**, *14*, 15595−15604.
(17) Wyss, K. M.; De Kleine, R. D.; Couvreur, R. L.; Kiziltas, A.; Mielewski, D. F.; Tour, J. M. Upcycling End-of-Life Vehicle Waste Plastic into Flash Graphene. *Commun. Eng.* **2022**, *1*, 3.
(18) Advincula, P. A.; Granja, V.; Wyss, K. M.; Algozeeb, W. A.; Chen, W.; Beckham, J. L.; Luong, D. X.; Higgs, C. F.; Tour, J. M. Waste Plastic- and Coke-Derived Flash Graphene as Lubricant Additives. *Carbon* **2023**, *203*, 876−885.
(19) Luong, D. X.; Bets, K. V.; Algozeeb, W. A.; Stanford, M. G.; Kittrell, C.; Chen, W.; Salvatierra, R. V.; Ren, M.; McHugh, E. A.; Advincula, P. A.; Wang, Z.; Bhatt, M.; Guo, H.; Mancevski, V.; Shahsavari, R.; Yakobson, B. I.; Tour, J. M. Gram-Scale Bottom-up Flash Graphene Synthesis. *Nature* **2020**, *577*, 647−651.
(20) Saadi, M. A. S. R.; Advincula, P. A.; Thakur, M. S. H.; Khater, A. Z.; Saad, S.; Zeraati, A. S.; Nabil, S. K.; Zinke, A.; Roy, S.; Lou, M.; Bheemasetti, S. N.; Al Bari, M. A.; Zheng, Y.; Beckham, J. L.; Gadhamshetty, V.; Vashisth, A.; Kibria, M. G.; Tour, J. M.; Ajayan, P. M.; Rahman, M. M. Sustainable Valorization of Asphaltenes via Flash Joule Heating. *Sci. Adv.* **2022**, *8*, No. eadd3555.
(21) Wu, Y.; Advincula, P. A.; Giraldo-Londoño, O.; Yu, Y.; Xie, Y.; Chen, Z.; Huang, G.; Tour, J. M.; Lin, J. Sustainable 3D Printing of Recyclable Biocomposite Empowered by Flash Graphene. *ACS Nano* **2022**, *16*, 17326−17335.
(22) Advincula, P. A.; Luong, D. X.; Chen, W.; Raghuraman, S.; Shahsavari, R.; Tour, J. M. Flash Graphene from Rubber Waste. *Carbon* **2021**, *178*, 649−656.
(23) Stanford, M. G.; Bets, K. V.; Luong, D. X.; Advincula, P. A.; Chen, W.; Li, J. T.; Wang, Z.; McHugh, E. A.; Algozeeb, W. A.; Yakobson, B. I.; Tour, J. M. Flash Graphene Morphologies. *ACS Nano* **2020**, *14*, 13691−13699.
(24) Advincula, P. A.; De Leon, A. C.; Rodier, B. J.; Kwon, J.; Advincula, R. C.; Pentzer, E. B. Accommodating Volume Change and Imparting Thermal Conductivity by Encapsulation of Phase Change Materials in Carbon Nanoparticles. *J. Mater. Chem. A* **2018**, *6*, 2461−2467.
(25) Wyss, K. M.; Li, J. T.; Advincula, P. A.; Bets, K. V.; Chen, W.; Eddy, L.; Silva, K. J.; Beckham, J. L.; Chen, J.; Meng, W.; Deng, B.; Nagarajaiah, S.; Yakobson, B. I.; Tour, J. M. Upcycling of Waste Plastic into Hybrid Carbon Nanomaterials. *Adv. Mater.* **2023**, *35*, 2209621.
(26) Advincula, P. A.; Beckham, J. L.; Choi, C. H.; Chen, W.; Han, Y.; Kosynkin, D. V.; Lathem, A.; Mayoral, A.; Yacaman, M. J.; Tour, J. M. Tunable Hybridized Morphologies Obtained through Flash Joule Heating of Carbon Nanotubes. *ACS Nano* **2023**, *17*, 2506−2516.
(27) Chen, W.; Li, J. T.; Wang, Z.; Algozeeb, W. A.; Luong, D. X.; Kittrell, C.; McHugh, E. A.; Advincula, P. A.; Wyss, K. M.; Beckham, J. L.; Stanford, M. G.; Jiang, B.; Tour, J. M. Ultrafast and Controllable Phase Evolution by Flash Joule Heating. *ACS Nano* **2021**, *15*, 11158−11167.
(28) Chen, W.; Ge, C.; Li, J. T.; Beckham, J. L.; Yuan, Z.; Wyss, K. M.; Advincula, P. A.; Eddy, L.; Kittrell, C.; Chen, J.; Luong, D. X.; Carter, R. A.; Tour, J. M. Heteroatom-Doped Flash Graphene. *ACS Nano* **2022**, *16*, 6646−6656.
(29) Chen, W.; Li, J. T.; Ge, C.; Yuan, Z.; Algozeeb, W. A.; Advincula, P. A.; Gao, G.; Chen, J.; Ling, K.; Choi, C. H.; McHugh, E. A.; Wyss, K. M.; Luong, D. X.; Wang, Z.; Han, Y.; Tour, J. M. Turbostratic Boron-Carbon-Nitrogen and Boron-Nitride by Flash Joule Heating. *Adv. Mater.* **2022**, *34*, 2202666.
(30) Chen, W.; Salvatierra, R. V.; Li, J. T.; Kittrell, C.; Beckham, J. L.; Wyss, K. M.; La, N.; Savas, P. E.; Ge, C.; Advincula, P. A.; Scotland, P.; Eddy, L.; Deng, B.; Yuan, Z.; Tour, J. M. Flash Recycling of Graphite Anodes. *Adv. Mater.* **2023**, *35*, 2207303.
(31) Deng, B.; Meng, W.; Advincula, P. A.; Eddy, L.; Ucak-Astarlioglu, M. G.; Wyss, K. M.; Chen, W.; Carter, R. A.; Li, G.; Cheng, Y.; Nagarajaiah, S.; Tour, J. M. Heavy Metal Removal from Coal Fly Ash for Low Carbon Footprint Cement. *Commun. Eng.* **2023**, *2*, 1−11.
(32) Bouckaert, S.; Pales, A. F.; McGlade, C.; Remme, U.; Wanner, B.; Varro, L.; D'Ambrosio, D.; Spencer, T. IEA Net Zero by 2050: A Roadmap for the Global Energy Sector. *Int. Energy Agency* 2021, 224.
(33) Beckham, J. L.; Wyss, K. M.; Xie, Y.; McHugh, E. A.; Li, J. T.; Advincula, P. A.; Chen, W.; Lin, J.; Tour, J. M. Machine Learning Guided Synthesis of Flash Graphene. *Adv. Mater.* **2022**, *34*, 2106506.
(34) Du, M.; Advincula, P. A.; Ding, X.; Tour, J. M.; Xiang, C. Coal-Based Carbon Nanomaterials: En Route to Clean Coal Conversion toward Net Zero CO_2. *Adv. Mater.* **2023**, *35*, 2300129.
(35) Advincula, P. A.; Meng, W.; Eddy, L. J.; Beckham, J. L.; Siqueira, I. R.; Luong, D. X.; Chen, W.; Pasquali, M.; Nagarajaiah, S.; Tour, J. M. Ultra-High Loading of Coal-Derived Flash Graphene Additives in Epoxy Composites. *Macromol. Mater. Eng.* **2023**, *308*, 2200640.
(36) Ai, Q.; Gao, L.; Huang, D.; Yang, J.; Fu, Q.; Zheng, X.; Liu, Y.; Qiao, L.; Weng, J.; Zheng, M. Non-Target and Target Analysis to Identify and Characterize Thiophenes in Soil from an Abandoned Coking Plant. *J. Hazard. Mater.* **2023**, *460*, No. 132444.
(37) Rudyka, V. I.; Soloviov, M. A.; Malyna, V. P. Innovations in Coke Production, Market Trends: Insights from the Eurocoke 2019 Summit. *Coke Chem.* **2019**, *62*, 267−279.
(38) Matyjaszek, M.; Wodarski, K.; Krzemień, A.; Escanciano García-Miranda, C.; Suárez Sánchez, A. Coking Coal Mining Investment: Boosting European Union's Raw Materials Initiative. *Resour. Policy* **2018**, *57*, 88−97.
(39) Commerce, U. S. D. of. Coal Data - *U.S. Energy Information Administration (EIA)* https://www.eia.gov/coal/production/quarterly/pdf/t17p01p1.pdf 2023.
(40) Xu, W.; Birbilis, N.; Sha, G.; Wang, Y.; Daniels, J. E.; Xiao, Y.; Ferry, M. A High-Specific-Strength and Corrosion-Resistant Magnesium Alloy. *Nat. Mater.* **2015**, *14*, 1229−1235.

(41) Challis, V. J.; Xu, X.; Zhang, L. C.; Roberts, A. P.; Grotowski, J. F.; Sercombe, T. B. High Specific Strength and Stiffness Structures Produced Using Selective Laser Melting. *Mater. Des.* **2014**, *63*, 783−788.
(42) Wu, Y. Y.; Que, L.; Cui, Z.; Lambert, P. Physical Properties of Concrete Containing Graphene Oxide Nanosheets. *Materials* **2019**, *12*, 1707.
(43) Pan, Z.; He, L.; Qiu, L.; Korayem, A. H.; Li, G.; Zhu, J. W.; Collins, F.; Li, D.; Duan, W. H.; Wang, M. C. Mechanical Properties and Microstructure of a Graphene Oxide-Cement Composite. *Cem. Concr. Compos.* **2015**, *58*, 140−147.
(44) Han, B.; Sun, S.; Ding, S.; Zhang, L.; Yu, X.; Ou, J. Review of Nanocarbon-Engineered Multifunctional Cementitious Composites. *Composites Part A* 2015, *1*, 69 81 Elsevier.
(45) Meng, W.; Khayat, K. H. Mechanical Properties of Ultra-High-Performance Concrete Enhanced with Graphite Nanoplatelets and Carbon Nanofibers. *Compos. Part B Eng.* **2016**, *107*, 113−122.
(46) Neville, G. B. *Concrete Manual: Based on the 2015 IBC and ACI 318−14*; ICC, 2015.

https://doi.org/10.1021/acsami.3c15156
ACS Appl. Mater. Interfaces 2024, 16, 1474−1481